

Available online at www.sciencedirect.com

ScienceDirect

www.elsevier.com/locate/jes

JES
JOURNAL OF
ENVIRONMENTAL
SCIENCES
www.jesc.ac.cn

Research Article

Environmental colloid behaviors of humic acid - Cadmium nanoparticles in aquatic environments

Ruyi Zheng^{1,2}, Jian Zhu^{1,2,*}, Peng Liao^{3,*}, Dengjun Wang⁴, Pan Wu^{1,2},
Wenjian Mao^{1,2}, Yuqin Zhang^{1,2}, Weiwei Wang^{1,2}

¹College of Resources and Environment Engineering, Key Laboratory of Karst Georesources and Environment, Ministry of Education, Guizhou University, Guiyang 550025, China

²Guizhou Karst Environmental Ecosystems Observation and Research Station, Ministry of Education, Guizhou University, Guiyang 550025, China

³State Key Laboratory of Environmental Geochemistry, Institute of Geochemistry, Chinese Academy of Science, Guiyang 550081, China

⁴School of Fisheries, Aquaculture and Aquatic Sciences, Auburn University, Auburn, AL 36849, USA

ARTICLE INFO

Article history:

Received 6 December 2023

Revised 22 February 2024

Accepted 22 February 2024

Available online 16 March 2024

Keywords:

HA-Cd(II) colloids

Colloid formation

Colloid aggregation

Transport

ABSTRACT

Humic acid (HA), a principal constituent of natural organic matter (NOM), manifests ubiquitously across diverse ecosystems and can significantly influence the environmental behaviors of Cd(II) in aquatic systems. Previous studies on NOM-Cd(II) interactions have primarily focused on the immobilization of Cd(II) solids, but little is known about the colloidal stability of organically complexed Cd(II) particles in the environment. In this study, we investigated the formation of HA-Cd(II) colloids and quantified their aggregation, stability, and transport behaviors in a saturated porous media representative of typical subsurface conditions. Results from batch experiments indicated that the relative quantity of HA-Cd(II) colloids increased with increasing C/Cd molar ratio and that the carboxyl functional groups of HA dominated the stability of HA-Cd(II) colloids. The results of correlation analysis between particle size, critical aggregation concentration (CCC), and zeta potential indicated that both Derjaguin-Landau-Verwey-Overbeek (DLVO) and non-DLVO interactions contributed to the enhanced colloidal stability of HA-Cd(II) colloids. Column results further confirmed that the stable HA-Cd(II) colloid can transport fast in a saturated media composed of clean sand. Together, this study provides new knowledge of the colloidal behaviors of NOM-Cd(II) nanoparticles, which is important for better understanding the ultimate cycling of Cd(II) in aquatic systems.

© 2024 The Research Center for Eco-Environmental Sciences, Chinese Academy of Sciences. Published by Elsevier B.V.

* Corresponding authors.

E-mails: jzhu@gzu.edu.cn (J. Zhu), liaopeng@mail.gyig.ac.cn (P. Liao).

Introduction

The element cadmium (Cd) is characterized by its high toxicity and mobility (Nies, 2003). Cd can enter into the environment through various pathways, including wastewater discharge, residue from mining and metallurgy, agricultural irrigation, phosphate fertilizer application, and automobile exhaust (Lucon et al., 2020; Yan et al., 2021; Yun et al., 2016). Cd is relatively non-biodegradable and can persist in the environment for extended periods (Lucon et al., 2020; Meng et al., 2024; Ni et al., 2016). The migration of Cd in aquatic systems is contingent upon its chemical form. Common Cd forms that can be migrated include water-dissolved Cd, non-specific adsorbed Cd, and organic-metal complexes (Crea et al., 2013; Hua et al., 2019; Zhao et al., 2022). Natural organic matter (NOM) is a mixture of organic compounds, which plays a critical role in the complexation and migration of Cd in the natural environment (Karimian et al., 2019; Li et al., 2022; Liu et al., 2021b; Zhang et al., 2020a). Thus far, many studies have focused on understanding the influence of NOM on the partitioning of Cd in soil or water by interacting with minerals or microorganisms to co-precipitate. (Chen et al., 2018; Li et al., 2020c; Qu et al., 2022; Zhou et al., 2020). Humic acid (HA), as a typical NOM, enhances the ability of Cd to form complex with its own oxygen-containing functional groups. This occurs through mechanisms like electrostatic interactions and microbial processes, thus reducing its bioavailability and leaching toxicity (Cao et al., 2021; Chen et al., 2022; Zhang et al., 2024; Zhong et al., 2023). Nevertheless, it is essential to underscore that the transformative effects witnessed in Cd partitioning cannot be solely attributed to the direct action of NOM. It has been reported that Cd(II) binds exclusively to humus in watersheds enriched with a wide range of soluble dissolved organic matter (SDOM) (Fan et al., 2023; Zhu et al., 2022a). This is attributed to the high proportion of carboxyl groups in the aromatic carbon of humus macromolecules and the possible formation of unique functional group compositions that alter the SDOM-Cd(II) binding pathway (Huang et al., 2022; Wen et al., 2022; Zhu et al., 2022a). However, there is a lack of information on the colloidal behaviors of HA-Cd(II) nanoparticles, leaving a critical knowledge gap in the ultimate fate and transport of Cd. Considering the risk of Cd-contaminated sites with high HA content (Fan et al., 2023; Lodygin et al., 2020; Maurer et al., 2012; Pan et al., 2023), it is crucial to understand the behaviors of Cd in the environment mediated by the stability of HA nanoparticles.

Colloid-facilitated contaminant transport is an important process governing the transport of heavy metal contaminants, including Cd, in subsurface environment (Bolan et al., 2014; Chotpantarat and Kiatvarangkul, 2018; Guan et al., 2018; Li et al., 2022, 2019; Liao et al., 2017, 2020; Yang et al., 2019a; Zhang et al., 2020b). It has been studied that kaolinite colloids promote the migration of Cu, Pb, and Zn ions (Won et al., 2019). The presence of HA can change the distribution and transport propensity of Fe and Cr in aerobic and anaerobic environments (Li et al., 2020b; Liao et al., 2020). Mounting field evidences highlight the prevalence of dissolved Cd(II) bound to a variety of organic colloidal ligands (e.g., humic substances) in aqueous and soil systems. Cd adsorption onto HA involves

multiple mechanisms, including ion exchange, electrostatic interactions, coprecipitation, and complexation. Notably, the complexation process is facilitated by the hydroxyl groups on the organic colloidal ligands surface, which interact with Cd through various bonding configurations, such as edge-sharing (coboundary) and corner-sharing (coangle) complexes. These interactions contribute to the diverse and dynamic nature of Cd binding in the organic colloidal ligands matrix (Fan et al., 2023; Gao et al., 2023; Tang et al., 2020; Tiberg et al., 2018; Zhou et al., 2020). HA can reduce Cd(II) mobility by recapturing Cd(II) to form a more stable component, lowering the bioavailability of Cd (Chen et al., 2018; Long et al., 2024; Xu et al., 2019). The formation of Cd(II) complex is thought to promote the dissolution of Cd-containing minerals through a series of reaction pathways (Han et al., 2024; Shen et al., 2022; Tiberg et al., 2018). Contrary to a growing body of research on Cd(II)-bearing minerals, little is known about the properties of NOM-Cd colloids in aqueous environments (Hoffmann et al., 2020). Thus, there is a need to elucidate the formation and other behaviors of HA-Cd(II) colloids for accurately understanding its fate and transport.

The aggregation of organic-metal colloids is an important mechanism to change the particle size distribution, particle interaction, and control their mass flux, migration and deposition (Meng et al., 2021; Sikder et al., 2020; Wu et al., 2022; Zhu et al., 2022b). A large number of studies have been conducted to induce the aggregation of nanoparticles by adding organic matter (humic acids, peptides, enzymes), inorganic electrolyte solutions (NaCl, CaCl₂, MgCl₂), changing light intensity, regulating pH, nanobubbles, and others (He et al., 2020; Liu et al., 2021a; Opitz et al., 2022; Su and Liu, 2017; You and Tseng, 2019). Furthermore, our recent work reported that the ratio of HA to metal is an imperative factor governing the aggregation of HA-metal colloids (Li et al., 2022, 2019; Liao et al., 2017). Mobile colloids can be considered as major players facilitating transport in low-solubility metallic water environments. The mobility of heavy metals such as U(VI), As(V) and Cr(III) in advective transport can be enhanced by forming organic-metal complexes with natural ligands (Li et al., 2022; Yang et al., 2019a; Yao et al., 2020). However, there is limited information on the colloidal chemistry of HA-Cd(II) nanoparticles, which limits our ability to fully assess Cd cycling.

The objective of this study was to investigate the formation, aggregation, and transport of HA-Cd(II) colloids in aqueous environments. To achieve this goal, HA-Cd(II) colloids were generated through batch experiments under a range of environmentally relevant conditions. Subsequently, a series of techniques such as Fourier Transform Infrared spectroscopy (FT-IR), X-ray Diffraction (XRD), X-ray photoelectron spectroscopy (XPS), and Transmission Electron Microscope (TEM) were employed to determine the nanoscale behaviors of colloids. Furthermore, laboratory-scale column experiments were conducted to assess the transport of HA-Cd(II) colloids in a porous media. This study offers a basic understanding of the behavior of cadmium nanoparticles in the presence of representative NOM components and provides promising avenue for quantitatively predicting the fate of trace metals related to other NOM-Cd(II) in aquatic environments.

1. Materials and methods

1.1. Materials

All reagent solutions were prepared using ultrapure water (resistivity >18.2 MΩ·cm, Milli-Q, Millipore). Cd(II) stock solution was prepared by dissolving 0.102 g of CdCl₂·5H₂O (>97%, Alfa Aesar) in 250 mL water to reach a concentration of 200 mg/L. Humic acid (HA; Sigma Aldrich) suspension was prepared by adding 1 g of dry powder in 200 mL deionized water and adjusting its pH to 10.5 using 0.1 and 5 mol/L NaOH. HA was selected as a model NOM compound in this study due to its previous use in organic-metal colloids studies (Li et al., 2022, 2019; Ma et al., 2018; Su et al., 2020; Wang et al., 2020; Yao et al., 2022, 2020), enabling comparisons with other research results. To avoid any photochemical reactions, the mixture was stirred on a magnetic stirrer for 24 hr in the dark and the resulting suspension was filtered through 0.45 μm nitrocellulose filters (PES). The total organic carbon (TOC) of the HA stock suspension was determined at 1726 ± 12 mg C/L using a TOC analyzer (Vario TOC, Elementar, Germany). Due to the strong correlation between HA and absorbance, the specific UV absorbance of HA was determined by diluting the HA stock solution to 0–64 mg C/L (SUVA254) and their UV absorbance at 420 nm was measured using a UV-vis spectrophotometer (Evolution 201, Thermo, USA) (Ma et al., 2018). Based on the linear relationship between colloid concentration and colloid absorbance, the linear equation for calculating colloid concentration was determined (Appendix A Fig. S1). Both stock suspensions were then used to create suspensions with different working concentrations for subsequent experiments.

1.2. Formation and characterization of HA-Cd(II) colloids

Batch experiments were conducted to investigate the impact of molar C/Cd ratios on HA-Cd(II) colloid formation in 100 mL blue-mouthed bottles wrapped in tin foil to prevent photochemical reactions. The pH of all solutions was maintained at 7.0±0.1 using 1 mmol/L NaOH and 1 mmol/L HCl. The HA-Cd(II) colloid formation experiment involved mixing fresh Cd(II) stock solution with an array of HA working suspensions at concentrations ranging from 0 to 64.3 mg C/L, resulting in an HA-Cd(II) colloid suspension with 5 mg/L Cd(II) and C/Cd molar ratios of 0–120, respectively. The mixture was then placed in an oscillator at 200 r/min for 12 hr or longer. The use of 5 mg/L Cd(II) to improve the analytical sensitivity and accuracy for studying the colloidal stability of organically complexed Cd(II). In reality, high concentrations of organically complexed Cd(II) (10 mg/L) can be present in natural and contaminated aquatic environments (Yang et al., 2023; Zhou et al., 2017). Repeated controlled experiments were conducted using HA suspension only without Cd addition. At the end of the experiment, samples were collected from the various reactors for chemical analysis, characterization, and subsequent aggregation experiments, which are described below.

The concentrations of Cd(II) and HA in different size fractions were initially determined through chemical analysis. In this study, colloids were defined as particles ranging from 10,000 Da (approximately 1–3 nm) to 0.45 μm (Li et al., 2019;

Liao et al., 2017, 2020). Samples passing through the 10,000 Da ultrafiltration membrane were considered as truly dissolved fraction, while those that remained on the 0.45 μm filter were classified as particulate species. The truly dissolved species of Cd(II) and HA were isolated from the sample by 10,000 Da (approximately < 1–3 nm) ultrafiltration membrane (EMD, Millipore) and 0.45 μm filter, respectively, while colloid (1–3 to 450 nm) and particulates (> 450 nm) were also collected. The Cd(II) concentration in each fraction was determined by atomic absorption spectrophotometer (AAS, Thermo, USA) after acidification with 5% HCl. The HA concentration in each fraction was quantified using a TOC analyzer described above.

The surface properties and crystalline structure of HA-Cd(II) colloids were characterized using Fourier transform infrared (Nicolet 6700, Thermo, USA) spectroscopy, X-ray photoelectron spectroscopy (Scientific K-Alpha, Thermo, USA), and powder X-ray diffraction (D8 Advance, BrukerAXS, Germany). The solid samples were obtained by freezing and drying. FT-IR spectra were recorded using the diffuse reflection attachment of the Nicolet 50 FT-IR instrument. XPS spectral analysis was performed with a 400 μm X-ray spot, and full spectrum and narrow spectrum sweep energies of 150 eV and 50 eV, respectively. The spectra were calibrated using C1s associated with graphitic carbon at 284.8 eV as a reference. XRD spectrum of powder samples was conducted using Cu target radiation acquisition under a tube current of 40 mA and tube voltage of 40 kV. The size distributions of HA-Cd(II) colloids were determined by dynamic light scattering (DLS) using a Zetasizer Nano (Zetasizer Nano, Malvern, UK). For each measurement, approximately 0.6 mL of the suspension was added to a polystyrene cuvette and analyzed immediately. The morphology of HA-Cd(II) colloids was imaged using a transmission electron microscope (JEM-F200, JEOL, Japan).

1.3. Aggregation of HA-Cd(II) colloids

The aggregation kinetic of HA-Cd(II) colloids was evaluated using a time-resolved DLS to monitor their mean hydrodynamic diameter over a wide range of electrolyte concentrations. Since the aggregation of HA-Cd(II) colloid was observed to be negligible at high monovalent cation concentrations (i.e., 1000 mmol/L NaCl, Appendix A Fig. S2), we considered aggregation as a function of divalent cations (Ca²⁺ and Mg²⁺). Ca²⁺ and Mg²⁺ were chosen as the representativeness for assessing the aggregation of engineered nanoparticles in water because of the high abundance in most natural aquifers (Dai et al., 2022; Gao et al., 2022; Li et al., 2022, 2019; Liao et al., 2017; Shams et al., 2020; Shao et al., 2021; Zhu et al., 2022b). At each measurement, an appropriate volume of HA-Cd(II) colloidal suspension (~1 mL) at a given C/Cd ratio was pipetted into the colorimetric dish. A predetermined amount of electrolyte and colloidal suspension is then quickly transferred to the cuvette to obtain the desired corresponding aggregation system. The initial change in the mean hydrodynamic diameter (D_h) was monitored every 15 sec over a 20 min period. Controlled experiments using HA (64 mg C/L) alone were performed with the same procedure and electrolyte concentration range. The aggregation kinetic of HA-Cd(II) colloids in this study was induced by the introduction of electrolytes (Ca²⁺ and Mg²⁺)

The aggregation rate (k) constant of HA-Cd(II) colloids was obtained by measuring the change of D_h with time in the specified time range (1200 sec).

$$k \propto \frac{1}{N_0} \left(\frac{dD_h(t)}{dt} \right)_{t \rightarrow 0} \quad (1)$$

where N_0 is the initial particle concentration in the suspension. By comparing the initial aggregation rate constant (k) under the given electrolyte concentration with the aggregation rate under the diffusion limited aggregation condition (k_{fast}), Then α can be determined as the ratio of the initial slope under the reaction constraint to the initial slope under the diffusion constraint.

$$\alpha = \frac{k}{k_{\text{fast}}} = \frac{\frac{1}{N_0} \left(\frac{dD_h(t)}{dt} \right)_{t \rightarrow 0}}{\frac{1}{N_0 \text{ fast}} \left(\frac{dD_h(t)}{dt} \right)_{t \rightarrow 0 \text{ fast}}} = \frac{\left(\frac{dD_h(t)}{dt} \right)_{t \rightarrow 0}}{\left(\frac{dD_h(t)}{dt} \right)_{t \rightarrow 0 \text{ fast}}} \quad (2)$$

The classical DLVO theory is often used to describe long-range interfacial forces in colloid systems (Derjaguin and Landau, 1941; Li et al., 2019; Verwey and Overbeek, 1947). DLVO theory can provide theoretical basis for studying the interaction mechanism and colloidal stability of HA-Cd(II) colloids under different conditions. In this study, an extended DLVO theory is used to describe the colloidal stability of HA-Cd(II) (Wang et al., 2020), with details providing in Appendix A Supplementary data.

1.4. Column experiments of HA-Cd(II) colloids

The transport of HA-Cd(II) colloids with HA concentrations of 13.4, 26.8 and 64.3 mg C/L in sand-packed saturated porous media was studied by column experiments. Quartz sand (99.3% SiO₂, average diameter 0.40 mm) was selected as a model porous medium. The sand was equilibrated with 1 mol/L NaOH and 10% H₂O₂ for 24 hr, and then cleaned several times with ultra-pure water to remove any metal oxide and particulate matter, and dried in the oven at 85 °C for 24 hr before use (Yao et al., 2020). The cylindrical plexiglass column (volume = 1.5 cm × 10 cm) was wet-filled with 26.0 g of cleaned quartz sand, and the porosity was measured to be 0.435. All column experiments were performed using a peristaltic pump in upward flow at a flow rate of 1 mL/min (Darcy flow rate = 0.19 cm/min). All columns and injection solutions were wrapped with tin foil to avoid any photochemical reactions. After filling the quartz sand column, a peristaltic pump (BT102S, Leaf) was used to continuously pump 10 pore volume (PV) of ultra-pure water (pH=7) upward, and then 10 pore volume concentration of 5 mmol/L NaCl solution was pumped into the quartz sand column to saturate the quartz sand column and normalize the pore water chemistry. Then, 14 PV of HA-Cd (II) influent suspension with the same background solution composition was injected into the column and eluted with 8 PV of ultrapure water (pH=7) background solution. Effluent samples were collected continuously using a fraction collector (BS-100A). At the end of each transport experiment, the column was evenly distributed into 10 fractions to determine the spatial distribution of Cd(II) retained in the column. Bromide (5 mg/L) was added to the packed column as a conservative tracer and used to calculate the hydrodynamic parameters of the column (Chotpantarat and Kiatvarangkul, 2018).

The model description and parameters are detailed in Appendix A Supplementary data.

2. Results and discussion

2.1. Formation of HA-Cd(II) colloids

The formation of HA-Cd(II) colloids largely depends on the molar ratio of C/Cd. Control experiments suggest that Cd(II) occurred as truly dissolved form without HA addition. The colloidal fraction of Cd(II) in the HA-Cd(II) suspension increased with increasing initial C/Cd molar ratio after 12 hr of equilibrium (Fig. 1a). The colloids (from 1-3 to 450 nm) fraction of Cd(II) in the HA-Cd(II) suspension increased linearly with the initial C/Cd molar ratio from 0 to 120, from 0% to a maximum value of 95.2%. This is accompanied by a decrease in truly dissolved Cd(II) (<1-3 nm) from 98.4% to 0.09%. Particulate Cd(II) (>450 nm) had a maximum value of 7.40% at C/Cd=10.

The variation of HA percentage under different sizes differed from that of Cd(II) under different initial C/Cd ratios (Fig. 1b). At high C/Cd (≥25), HA mainly existed in colloidal form, and a portion of dissolved HA could be attributed to its solubility. At C/Cd=3-25, the truly dissolved and particulate HA contents decreased by 25.3% and 29.98%, respectively, corresponding to an increase in the colloidal fraction. HA mainly existed in the colloidal fraction in the absence of Cd(II), and the difference in HA size distribution before and after reaction with Cd(II) was attributed to the interaction of Cd(II) with HA. At low C/Cd (≤10), a dramatic increase in truly dissolved HA was observed due to HA complexation with truly dissolved Cd(II) via ligand exchange mechanisms (Zhang et al., 2020a), which lowered the colloidal HA fraction. Thus, the formation of HA-Cd(II) colloids could be attributed to the complexation of truly dissolved Cd(II) by the oxygen-containing functional group of HA.

The binding capacity of HA to truly dissolved Cd was evaluated by analyzing the C/Cd ratio of the true colloidal component of Cd(II) in the equilibrated HA-Cd(II) suspension (Fig. 1c). The colloid fraction of Cd(II) after equilibrium was positively correlated with the initial C/Cd molar ratio. At low initial C/Cd molar ratios (e.g., C/Cd<25), the colloidal HA component/the colloidal Cd(II) component in the HA-Cd(II) suspension was 1.87 times higher than that of the initial C/Cd, and the colloid fraction of Cd(II) accounted for 44.2% of the system concentration. At high C/Cd molar ratios (C/Cd=120), Cd(II) was almost completely complexed with HA, the ratio of colloidal C/Cd to the initial C/Cd is close to 1, indicating that Cd(II) had a higher affinity for HA compared to Mn (Li et al., 2019). Additionally, the ratio of the $K_{\text{Cd(II)-Sol.HA}}/K_{\text{Cd(II)-Coll.HA}}$ constant between Cd(II) bound by truly dissolved HA and Cd(II) bound by colloidal HA showed that the ratio was less than 1 until C/Cd > 50, suggesting that truly dissolved HA(<1-3 nm) had a higher affinity for Cd(II) at low C/Cd.

The hydrodynamic diameter of the suspension containing only HA at different C/Cd ranges from 160 to 180 nm. The average hydrodynamic diameter distribution of the HA-Cd(II) suspension at different C/Cd ratios ranged from 220 to 400 nm (Fig. 1d). After C/Cd=25, the change in hydrodynamic diameter was inversely proportional to the Cd(II) colloids, and the

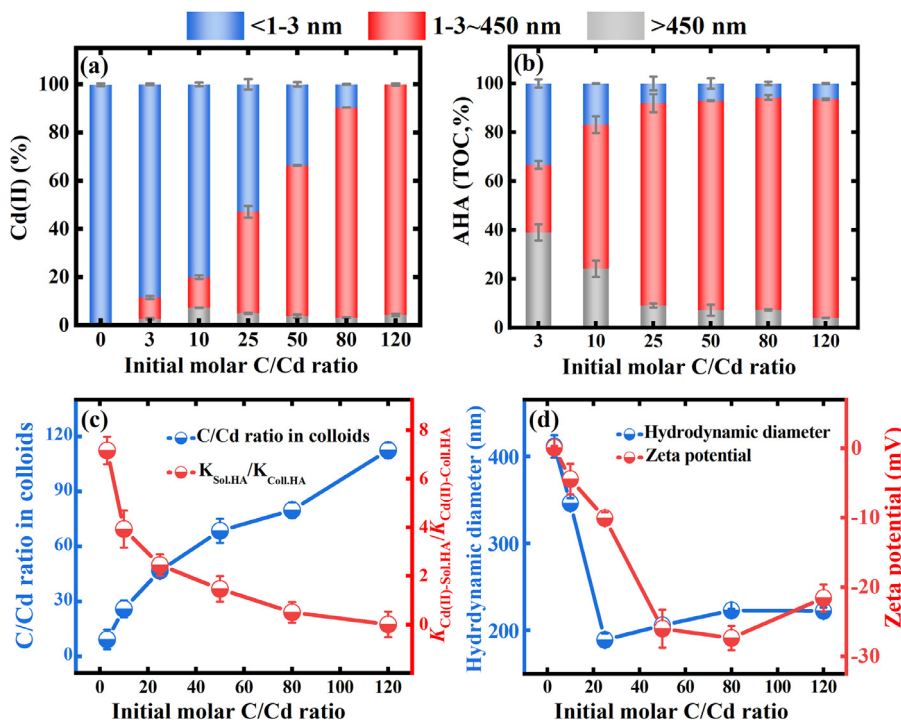


Fig. 1 – Formation of HA-Cd(II) colloids. Percentage of (a) Cd(II) and (b) HA concentrations in different size fractions at steady-state conditions as a function of initial C/Cd molar ratios. (c) The ratio of C/Cd in colloids and the evaluated $K_{\text{Cd(II)-Sol.HA}}/K_{\text{Cd(II)-Coll.HA}}$ as a function of initial C/Cd molar ratios and (d) Z-averaged hydrodynamic diameter and zeta potential of HA-Cd(II) as a function of initial C/Cd molar ratios. Each data point refers to the mean value of 9 measurements of duplicate samples. Error bars represent standard deviations.

colloidal fraction of HA was close to the peak. The zeta potential of the HA-Cd(II) colloids became more negative with the increase in molar C/Cd ratio and then tended to be stable. This is in contrast to the zeta potential of HA alone, which did not change significantly across different concentration ranges. Also, the hydrodynamic diameter of HA suspension for different concentration gradients was similar, ranging from 160 to 180 nm.

2.2. Characterization of HA-Cd(II) colloids

FT-IR was utilized to probe the surface functional groups of HA and HA-Cd(II) (Fig. 2a). The band at 3422 cm^{-1} was attributed to the stretching vibration of water molecules or phenolic hydroxyl groups, and the absorption band of $-\text{CH}_2$ appeared at approximately 2919 cm^{-1} (Fei et al., 2023; Yin et al., 2021). The effect of sorption was observed as a shift in the $\text{C}=\text{C}/\text{C}=\text{O}$ stretching vibration peak from 1612 cm^{-1} to 1584 cm^{-1} , and the characteristic $\text{C}=\text{O}$ (indicating $-\text{COO}^-$) peak at 1400 cm^{-1} shifted to the vicinity of 1385 cm^{-1} . This band vibration was typically attributed to the interaction between the carbon-oxygen double bond and metal (Chang et al., 2019; Cuong et al., 2021). Additionally, changes in the intensity of certain bands were observed. The intensity of the 1095 cm^{-1} band, associated with C-O groups, and the 538 cm^{-1} band, significantly decreased. These spectral changes collectively indicate that the complexation of Cd(II) with HA resulted in alterations to the

configuration of oxygen-containing functional groups within HA. XRD analysis showed good crystallinity and several new peaks at 2θ of 15.12° and 24.98° corresponding to the presence of Cd(II) crystals (JCPDS card number: 27-0073) (Fig. 2b) (Li et al., 2020a; Wang et al., 2022), which further demonstrated the complexation of Cd(II) with HA.

The full spectrum of HA and HA-Cd(II) was presented in Fig. 2c. XPS typically characterizes the top-surface (e.g., 1-10 nm) properties of HA-Cd(II) colloids. XPS spectra of Cd3d, C1s, and O1s were shown in Fig. 2d-f. The Cd3d peaks at 406.36 and 413.21 eV for HA-Cd(II) corresponded to the formation of O-Cd and Cd(OH)₂ (Yin et al., 2021), respectively. The C1s peaked at 284.78, 285.62, 286.78, and 288.47 eV, representing C-C, C-O, carbonyl C=O, and carboxyl -COOR groups, respectively (Wang et al., 2022), which were also confirmed by the FT-IR results described above. After complexation, the relative contents of C-C and C-O increased by 2.59% and 4.50%, respectively, while the contents of C=O and -COO decreased by 5.80% and 1.33%, respectively. The main O1s was deconvoluted into four peaks: hydroxy-bound metal (M-OH), surface hydroxyl (C-OH), metal oxide (M-O), and adsorbed water (H₂O) (Li et al., 2020a), with binding energies of 530.37, 531.37, 532.46, 533.32 eV, respectively. The relative content of M-O increased significantly from 23.3% to 36.8%, while the relative content of C-OH decreased significantly from 60.9% to 45.2%, indicating the formation of hydroxyl-bonded metal (Chang et al., 2019; Wang et al., 2022). These results indicated that in addition to substituting with the surface hydroxyl group to form hydroxy-

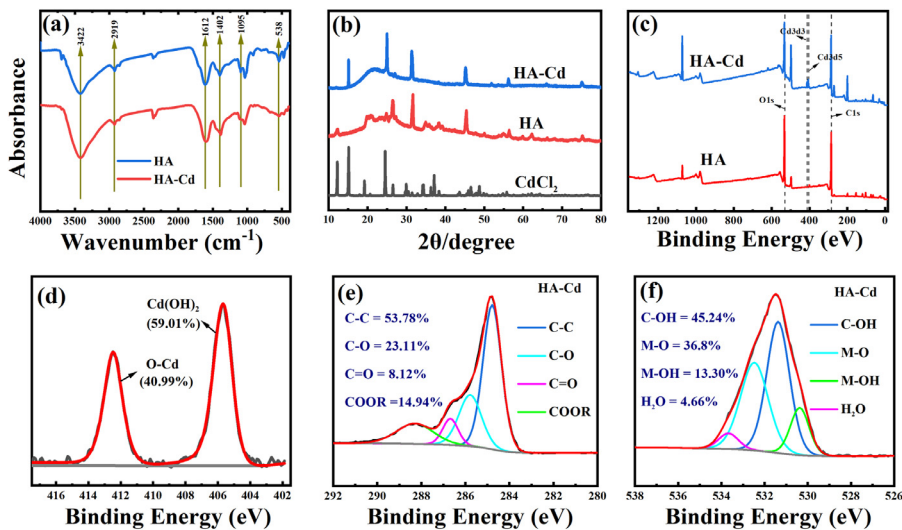


Fig. 2 – Characterization of HA-Cd(II) colloids. (a) FT-IR spectra of HA-Cd(II) colloids and individual AHA (b) XRD patterns of HA-Cd(II) colloids, individual HA and CdCl₂. The values of 2θ are those for copper Ka X-rays. (c) XPS full spectrum scanning of HA-Cd(II) and HA. The fine spectrum of (d) Cd3d, (e) C1s, and (f) O1s in HA-Cd(II) colloids.

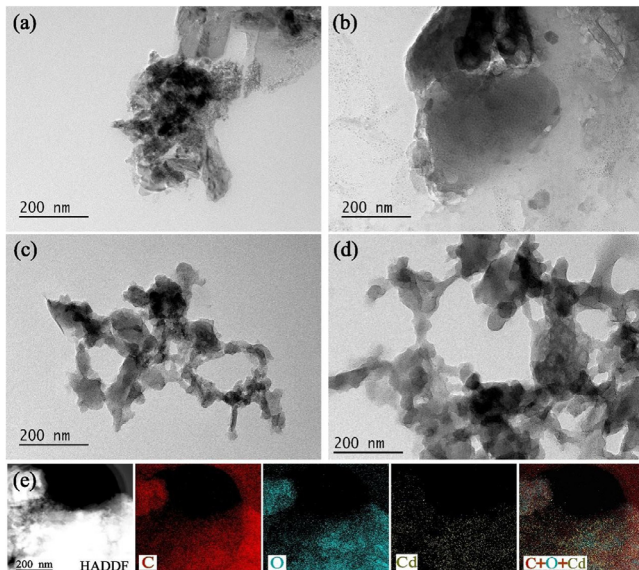


Fig. 3 – Morphology and microstructure of HA-Cd(II) colloids with different initial C/Cd molar ratios: (a) High-resolution HAADF-STEM images of C/Cd = 10, (b) C/Cd = 25 (c) C/Cd = 50, and (d) C/Cd = 120. (e) HA-Cd(II) colloids and the corresponding high-resolution EDS elemental mappings of C, O, and Cd, and color overlays. HA-Cd(II) colloids were imaged at an initial molar C/Cd ratio of 120.

bonded metal, Cd(II) may also interact with the carboxyl and carbonyl groups to form hydroxy-bonded metal.

Furthermore, TEM images revealed that the size and morphology of HA-Cd(II) colloid were affected by the change in C/Cd molar ratio (Fig. 3). At low C/Cd molar ratios, HA-Cd(II) colloids exhibited a large bulk structure. As C/Cd increased, the ring structure became more apparent (Fig. 3a-d). High-

resolution (5 nm and 20 nm) and large-size (0.5 μm and 1 μm) images showed that HA-Cd colloid still has a very thin sheet structure at C/Cd=120 (Appendix A Fig. S5). Similar results were observed for NOM-Mn(III) colloids formed in aquatic systems (Li et al., 2022, 2019; Myneni et al., 1999). The high-angle annular dark-field HAADF-TEM images show the close association of Cd and carbon at nanoscale, supporting the formation of HA-Cd(II) nanoparticles (Fig. 3e).

2.3. Aggregation of HA-Cd(II) colloids

The colloidal aggregation rate was evaluated by inducing colloid aggregation with appropriate monovalent and divalent metal cationic electrolyte concentrations (Fig. 4). The concentration of NaCl electrolyte had little effect on the aggregation of HA-Cd(II) colloids (Appendix A Fig. S2). Low concentrations of CaCl₂ and MgCl₂ were also unfavorable for the aggregation of HA-Cd(II) colloids. Comparing the aggregation behavior of colloids in Ca²⁺ and Mg²⁺ with the same initial C/Cd, it was found that Ca²⁺ had a lower coagulation value, and the induced aggregation effect on the hydrodynamic diameter was larger and the rate was faster, indicating that HA-Cd(II) colloids were sensitive to Ca²⁺ cation. This could be attributed to the specific adsorption ability of Ca²⁺ ion known as the “bridging effect” (Chen and Elim-elech, 2007; Gutierrez and Nguyen, 2012). Similar observations had been reported for the aggregation of other binary colloids or nanoparticles such as nano-activated carbon colloids, cerium oxide nanoparticles, and higher-order fullerene clusters (Aich et al., 2016; Li et al., 2019, 2020c; Liao et al., 2017; Shao et al., 2021).

The results demonstrated that HA-Cd(II) colloid formation occurred at different C/Cd ratios, and different HA-Cd(II) colloids in CaCl₂ and MgCl₂ exhibited distinct reaction-limited aggregation (RLA) and diffusion-limited aggregation (DLA) mechanisms. The aggregation and diffusion behavior

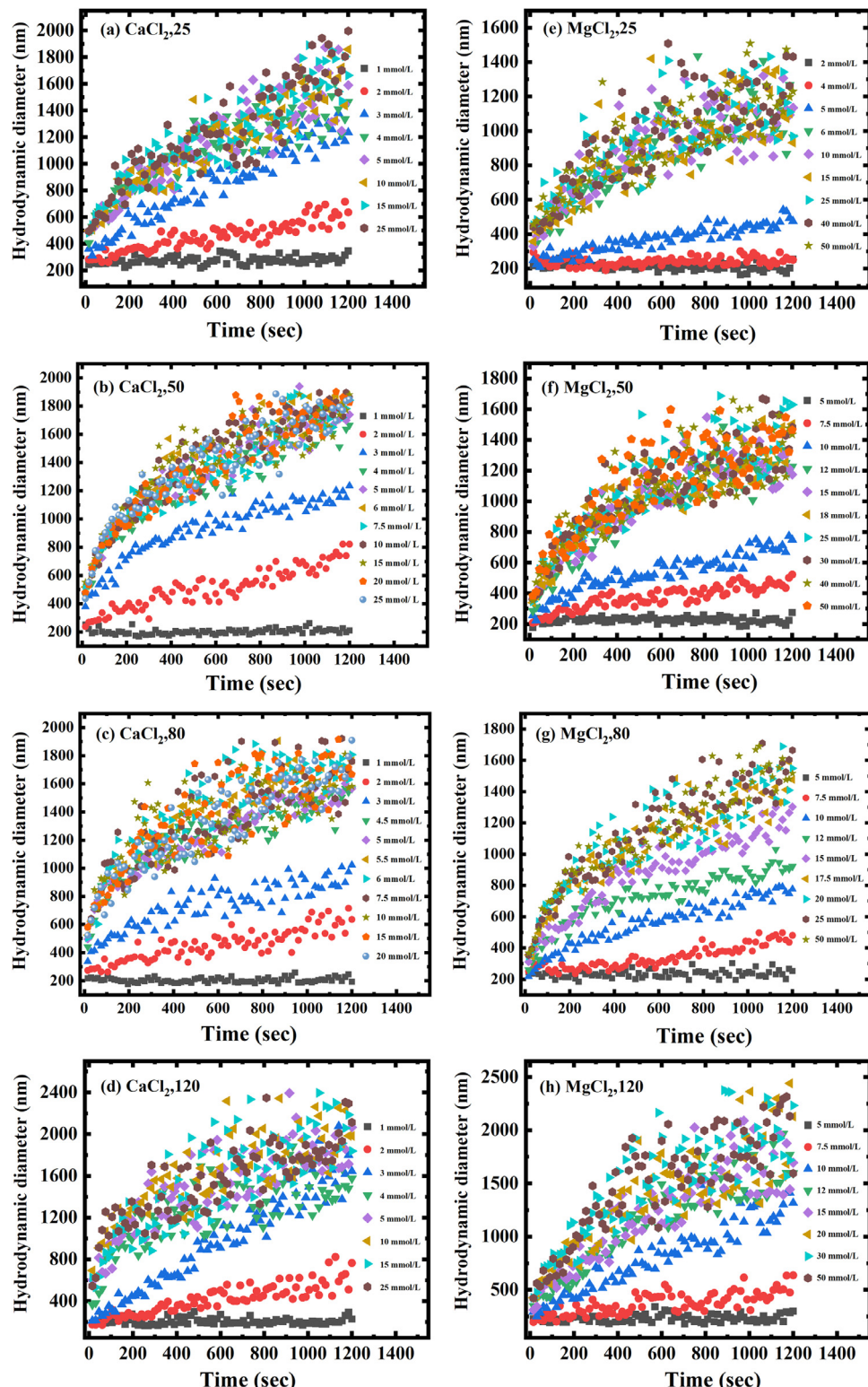


Fig. 4 – Aggregation kinetics of HA-Cd(II) colloids at C/Cd ratios = 25, 50, 80, and 120 under (a-d) Ca^{2+} and (e-h) Mg^{2+} . Hydrodynamic diameter measurements were made every 15 sec and 80 measurements were made in 20 min.

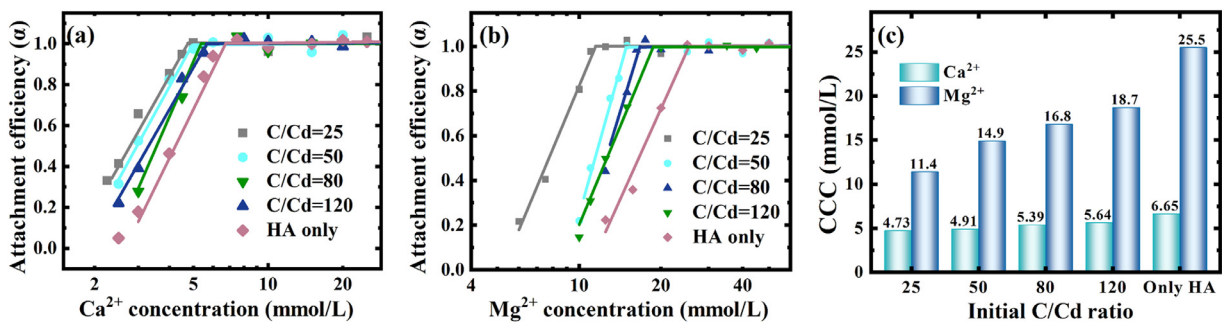


Fig. 5 – Attachment efficiency of HA-Cd(II) colloids at different C/Cd molar ratios as a function of (a) Ca^{2+} and (b) Mg^{2+} concentration at pH 7.0, and the corresponding critical coagulation concentration (CCC) is summarized in (c).

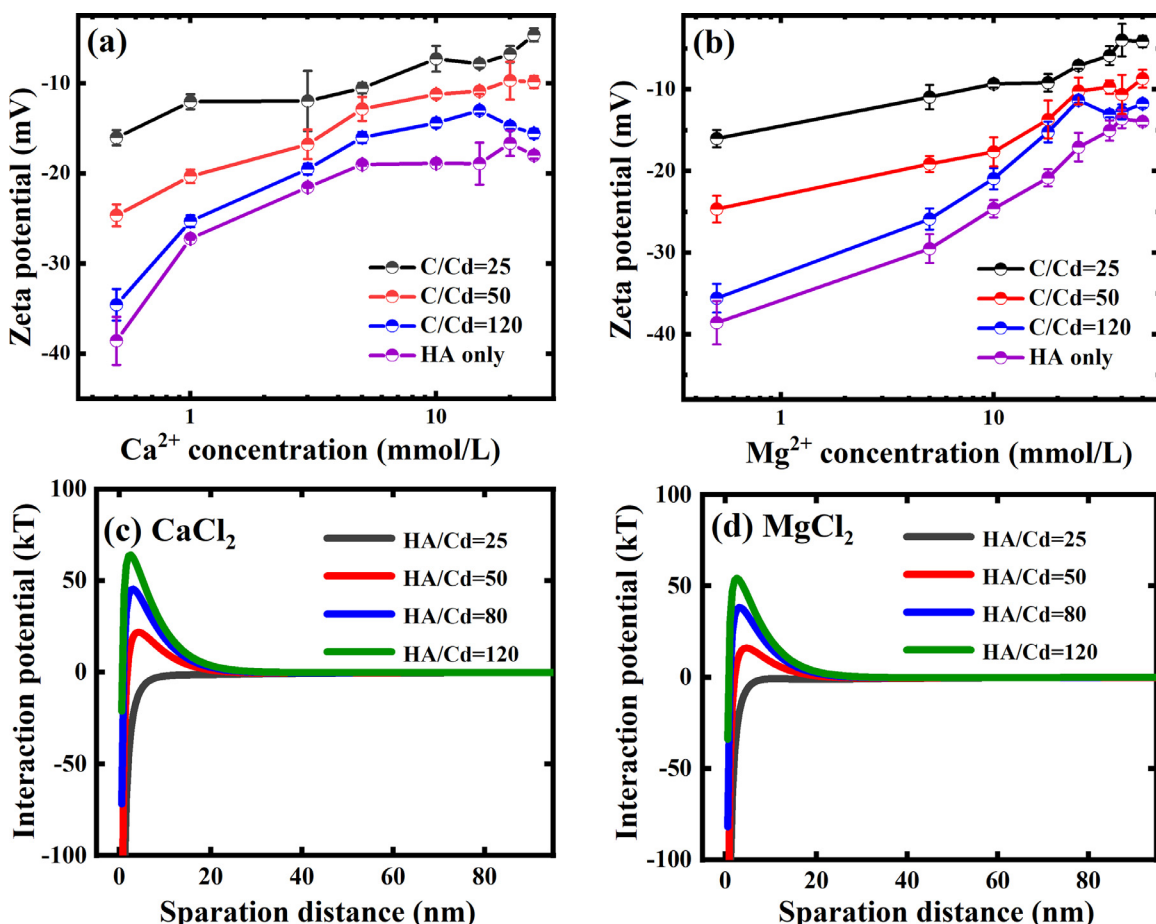


Fig. 6 – (a,b) Zeta potentials of different C/Cd molar ratios of HA-Cd(II) colloids over a range of (a) Ca^{2+} and (b) Mg^{2+} concentrations at pH 7.0. (c, d) Calculated interaction energy as a function of initial molar C/Cd ratios in the presence of 1 mmol/L (c) CaCl_2 and (d) MgCl_2 , at pH 7.0. The separation distance is from 0 to 100 nm.

of HA-Cd(II) colloids at different concentrations followed the classical Derjaguin-Landau-Verwey-Overbeek (DLVO) theory (Derjaguin and Landau, 1941; Verwey and Overbeek, 1947; Yang et al., 2019b). The critical coagulation concentration (CCC) is an indicator for the quantitative evaluation and comparison of colloidal stability of a colloid. At low electrolyte concentrations, the increase in salt concentration neutralized the surface charge of the HA colloids, resulting in a de-

crease in the negative zeta potential of the HA-Cd(II) colloids. This effectively reduced the electrostatic energy barrier between colloids, resulting in an increased particle-particle adhesion efficiency. When the electrolyte concentration exceeded the CCC, the repulsive force was completely eliminated, and the changes in hydrodynamic diameter and adhesion efficiency were independent on the salt concentration (Chen and Huang, 2017; Liu et al., 2020; Shams et al., 2020).

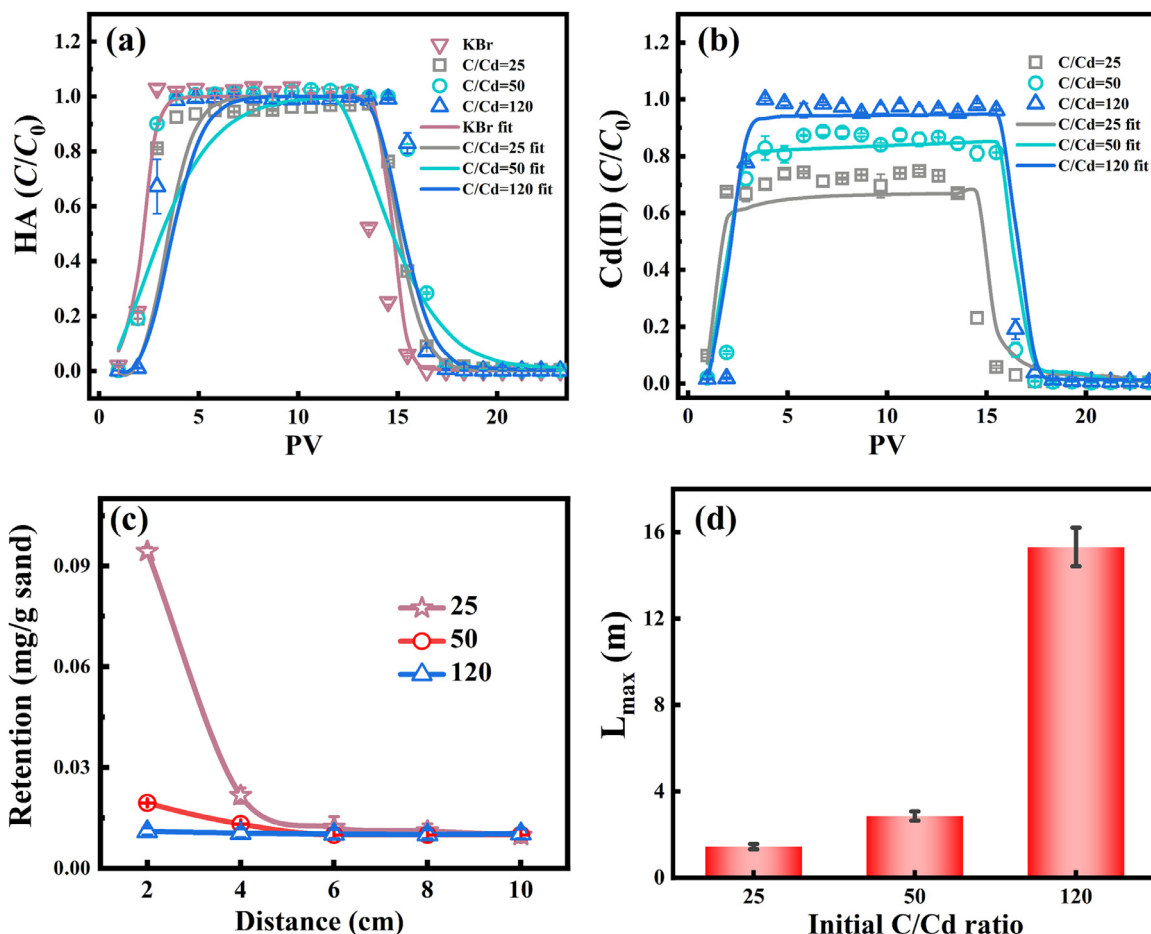


Fig. 7 – (a, b) Penetration curves of HA-Cd colloids in saturated aqueous porous media with pH 7.0. The breakthrough curve shows the normalized effluent concentration C/C_0 (where C and C_0 are the effluent concentrations of (a) HA or (b) Cd(II) in the HA-Cd suspension as a function of pore volume (PV), respectively. (c) deposition curves of Cd(II) for HA-Cd (II) colloid and larger particles at molar C/Cd ratios of 25, 50 and 120. (d) The maximum transport distance of HA-Cd(II) colloid as a function of the C/Cd molar ratio. Error bars indicate the standard deviation of repeated measures. Each error bar has five parallel data error results.

The HA-Cd(II) colloids exhibited stronger stability at high C/Cd ratios, resulting in higher CCC values. For instance, the CCC value of HA-Cd(II) colloids increased from 4.73 to 6.65 mmol/L when the initial molar C/Cd ratio increased from 25 to 120 in the presence of Ca^{2+} (Fig. 5). Similarly, when the initial molar C/Cd ratio increased from 25 to 120 in the presence of Mg^{2+} , the CCC value increased from 11.4 to 18.7 mmol/L. The enhanced stability of HA-Cd(II) colloids at high C/Cd ratios could be attributed to the presence of a large number of carboxyl groups, which provided stronger electronegativity to enhance the surface charge density.

Based on the classical DLVO theory, the relationship between zeta potential and CCC was approximated by relating the zeta potential to the CCC, and based on the surface change measurements, it was shown that there is a strong correlation between the concentration and type of the thus further electrolyte solution and the CCC. In addition, we found that when the potential of the suspension corresponding to the CCC value was exceeded, the potential did not change signif-

icantly, regardless of the type of electrolyte added, even with a significant increase in electrolyte concentration. Similar observations were reported for NOM-Mn(III) colloid and NOM-Cr(III) colloid (Li et al., 2020b, 2019), this may be attributed to the diffusion-limited aggregation (DLA) mechanism exhibited by HA-Cd(II) colloids, the increase in cation concentration is accompanied by an increase in zeta potential as one moves from a low to a high electrolyte concentration, and for a short period of time, the complexation of Ca^{2+} or Mg^{2+} with HA can form intramolecular and/or intermolecular bridges between neighboring colloids, compressing the thickness of the bilayer and thus increasing the attractiveness of the particles (Aich et al., 2016; Li et al., 2022, 2019). attraction, leading to an increase in colloid aggregation rate and size. When the electrolyte concentration is greater than CCC, the combined effect of cation charge screening, complexation and bridging reaches equilibrium, and the change of the thickness of the bilayer is small (Gao et al., 2022). Moreover, the zeta potential, which is the shear surface potential of the charged colloid, is

about 3.1–6.0 times lower than the surface potential (the potential of the original plane of the diffusion layer), and the effect of ions on the surface properties of the particles can be reflected more easily in the surface potential than in the zeta potential. Relatively higher electrolyte concentrations do not cause a significant change in zeta potential after reaching CCC (Duman and Tunç, 2009; Wang et al., 2013).

To provide a more comprehensive explanation of the observed results, the DLVO interaction energy was calculated (Fig. 6c and d). The results showed that HA-Cd(II) colloids with high C/Cd ratios had a higher repulsion energy barrier, indicating greater colloidal stability. The higher repulsion barrier with Mg at the same C/Cd ratio also suggested that Mg^{2+} had a stronger effect on the aggregation of HA-Cd(II) colloids.

2.4. Transport of HA-Cd(II) colloids

The concentration changes of HA and Cd(II) flowing out and deposited in the column revealed the transport of HA-Cd(II) colloid in porous medium (Fig. 7). The experimental results showed that the molar C/Cd ratio had a significant effect on the migration and deposition of Cd(II) colloids in a sand-packed column. With the increase of C/Cd, the breakthrough concentration of HA did not change significantly ($M_{eff} = 95.4\%–100.0\%$) under the same experimental conditions (Fig. 7a). High breakthrough concentration of Cd was reached, with M_{eff} ranging from 72.7% to 97.0% (Fig. 7b). The deposition profile further showed that most of the deposited Cd(II) was retained in the first half of the column (distance < 4 cm), and decreased significantly with increasing column depth (Fig. 7c). The particle size of the effluent was determined, and it was found that there was no significant change. At molar C/Cd ratio of 120, the breakthrough time of Cd(II) (~ 2.91 PV) was consistent with the breakthrough time of tracer (KBr) under the same conditions, confirming the high mobility of HA-Cd(II) colloids in the sand column, and further suggested that HA-Cd(II) colloid also has good migration ability in natural water environment. The enhanced transport of HA-Cd(II) colloids at high C/Cd ratios might be attributed to the mechanisms of electrostatic and steric repulsion interactions. Due to the higher repulsive potential of 56.3 KT (Ca^{2+}) and 64.1 KT (Mg^{2+}) at a C/Cd ratio of 120, the HA-Cd(II) colloid is more stable in the environment than at a C/Cd ratio of 25 where the repulsive potential is -0.786 KT and -0.827 KT (Fig. 6c and d), maintaining the consistent transport of the colloid.

We also evaluate the transport distance (L_{max}) using colloid filtration theory. Results demonstrate that even at relatively low C/Cd ratio of 25, the L_{max} was calculated to be ~1.44 m (Fig. 7d), which is a long distance in the subsurface environment. This indicates the significance of HA-Cd(II) colloids in promoting Cd(II) transport in porous media.

3. Conclusions

In this work, we systematically investigate the formation, aggregation, and transport behavior of HA-Cd(II) colloids under environmentally relevant conditions and quantify their colloidal behaviors through DLVO theory. The formation and stability of HA-Cd(II) colloids increased with increasing C/Cd ra-

tio, which could be attributed to the increase of surface electronegative functional groups. FT-IR and XPS characterization confirmed that Cd(II) formed the Cd-O bond by interacting with the O atom in the carbon-oxygen double bond. Common divalent cations were used to induce aggregation and investigate the stability of colloids in natural water samples. HA-Cd(II) colloids exhibited different interaction modes with different cations, resulting in differences in CCC values. Column results further confirmed that once colloidal Cd(II) was formed, it could travel a long distance during advective transport in media sand column. These results emphasize the importance of HA in organic-rich systems for influencing the environmental behavior of Cd(II) and provide new knowledge on the formation and transport of Cd(II) colloids in aquatic systems.

Declaration of Competing Interest

The authors declare that they have no known competing financial interests or personal relationships that could have appeared to influence the work reported in this paper.

Acknowledgments

This work was supported by Guizhou Science Cooperation Platform Talents (No. [GCC\[2023\]045](#)), the National Natural Science Foundation of China (Nos. [42267030](#) and [42177237](#)), the Innovation and Entrepreneurship Talents of Guizhou Province (No. [GZQ202208091](#)), the Science and Technology Planning Project of Guizhou Province (Qian Ke He Zhi Cheng, [2022–217](#)), the Science and Technology Planning Project of Guizhou Province (Qian Ke He Cheng Guo, [2023–006](#)).

Appendix A Supplementary data

Supplementary material associated with this article can be found, in the online version, at [doi:10.1016/j.jes.2024.02.015](https://doi.org/10.1016/j.jes.2024.02.015).

REFERENCE

- Aich, N., Boateng, L.K., Sabaraya, I.V., Das, D., Flora, J.R., Saleh, N.B., 2016. Aggregation kinetics of higher-order fullerene clusters in aquatic systems. *Environ. Sci. Technol.* 50, 3562–3571.
- Bolan, N., Kunhikrishnan, A., Thangarajan, R., Kumpiene, J., Park, J., Makino, T., et al., 2014. Remediation of heavy metal(lloid)s contaminated soils—to mobilize or to immobilize ? *J. Hazard. Mater.* 266, 141–166.
- Cao, Y., Wang, X., Zhang, X., Misselbrook, T., Bai, Z., Ma, L., 2021. An electric field immobilizes heavy metals through promoting combination with humic substances during composting. *Bioresour. Technol.* 330, 124996.
- Chang, R., Sohi, S.P., Jing, F., Liu, Y., Chen, J., 2019. A comparative study on biochar properties and Cd adsorption behavior under effects of ageing processes of leaching, acidification and oxidation. *Environ. Pollut.* 254, 113123.
- Chen, C., Huang, W., 2017. Aggregation kinetics of diesel soot nanoparticles in wet environments. *Environ. Sci. Technol.* 51, 2077–2086.

- Chen, K.L., Elimelech, M., 2007. Influence of humic acid on the aggregation kinetics of fullerene (C_{60}) nanoparticles in monovalent and divalent electrolyte solutions. *J. Colloid Interface Sci.* 309, 126–134.
- Chen, X., Du, Z., Liu, D., Wang, L., Pan, C., Wei, Z., et al., 2022. Biochar mitigates the biotoxicity of heavy metals in livestock manure during composting. *Biochar* 4.
- Chen, Y., Ma, J., Li, Y., Weng, L., 2018. Enhanced cadmium immobilization in saturated media by gradual stabilization of goethite in the presence of humic acid with increasing pH. *Sci. Total Environ.* 648, 358–366.
- Chotpantarat, S., Kiatvarangkul, N., 2018. Facilitated transport of cadmium with montmorillonite KSF colloids under different pH conditions in water-saturated sand columns: experiment and transport modeling. *Water Res.* 146, 216–231.
- Crea, F., Foti, C., Milea, D., Sammartano, S., 2013. Speciation of cadmium in the environment. *Met. Ions Life Sci.*
- Cuong, D.V., Wu, P.C., Chen, L.I., Hou, C.H., 2021. Active MnO_2 /biochar composite for efficient As(III) removal: Insight into the mechanisms of redox transformation and adsorption. *Water Res.* 188, 116495.
- Dai, H., Han, T., Cui, J., Li, X., Abbasi, H.N., Wang, X., et al., 2022. Stability, aggregation, and sedimentation behaviors of typical nano metal oxide particles in aqueous environment. *J. Environ. Manage.* 316, 115217.
- Derjaguin, B.V., Landau, L., 1941. Theory of the stability of strongly charged lyophobic sols and of the adhesion of strongly charged particles in solutions of electrolytes. *Acta phys. chim. URSS* 14, 733–762.
- Duman, O., Tunç, S., 2009. Electrokinetic and rheological properties of Na-bentonite in some electrolyte solutions. *Microporous Mesoporous Mater.* 117, 331–338.
- Fan, T., Yao, X., Sun, Z., Sang, D., Liu, L., Deng, H., et al., 2023. Properties and metal binding behaviors of sediment dissolved organic matter (SDOM) in lakes with different trophic states along the Yangtze River Basin: a comparison and summary. *Water Res.* 231, 119605.
- Fei, J., Cui, J., Wang, B., Xie, H., Wang, C., Zhao, Y., et al., 2023. Co-transport of degradable microplastics with Cd(II) in saturated porous media: synergistic effects of strong adsorption affinity and high mobility. *Environ. Pollut.* 330, 121804.
- Gao, X., Kou, Q., Ren, K., Zuo, Y., Xu, Y., Zhang, Y., et al., 2022. Quantitative characterization of non-DILO factors in the aggregation of black soil colloids. *Sci. Rep.* 12.
- Gao, Y., Tong, H., Zhao, Z., Cheng, N., Wu, P., 2023. Effects of Fe oxides and their redox cycling on Cd activity in paddy soils: a review. *J. Hazard. Mater.* 456, 131665.
- Guan, Z., Tang, X.Y., Nishimura, T., Katou, H., Liu, H-Y., Qing, J., 2018. Surfactant-enhanced flushing enhances colloid transport and alters macroporosity in diesel-contaminated soil. *J. Environ. Sci.* 64, 197–206.
- Gutierrez, L., Nguyen, T.H., 2012. Interactions between rotavirus and Suwannee river organic matter: aggregation, deposition, and adhesion force measurement. *Environ. Sci. Technol.* 46, 8705–8713.
- Han, B., Liu, J., Zhu, R., Chen, Q., 2024. Clay minerals inhibit the release of Cd(II) during the phase transformation of Cd(II)-ferrihydrite coprecipitates. *J. Hazard. Mater.* 462, 132723.
- He, H., Shi, X., Wang, J., Wang, X., Wang, Q., Yu, D., et al., 2020. Reactive oxygen species-induced aggregation of nanzymes for neuron injury. *ACS Appl Mater Interfaces* 12, 209–216.
- Hoffmann, K., Christl, I., Kaegi, R., Kretzschmar, R., 2020. Effects of natural organic matter (NOM), metal-to-sulfide ratio and Mn^{2+} on cadmium sulfide nanoparticle growth and colloidal stability. *Environ. Sci. Nano.* 7, 3385–3404.
- Hua, X., Huang, X., Tian, J., Dong, D., Liang, D., Guo, Z., 2019. Migration and distribution of cadmium in aquatic environment: the important role of natural biofilms. *Sci. Total Environ.* 670, 478–485.
- Huang, M., Zhou, M., Li, Z., Ding, X., Wen, J., Jin, C., et al., 2022. How do drying-wetting cycles influence availability of heavy metals in sediment? A perspective from DOM molecular composition. *Water Res.* 220, 118671.
- Karimian, N., Burton, E.D., Johnston, S.G., Hockmann, K., Choppala, G., 2019. Humic acid impacts antimony partitioning and speciation during iron(II)-induced ferrihydrite transformation. *Sci. Total Environ.* 683, 399–410.
- Li, A.Y., Deng, H., Jiang, Y.H., Ye, C.H., Yu, B.G., Zhou, X.L., et al., 2020a. Superefficient removal of heavy metals from wastewater by mg-loaded biochars: adsorption characteristics and removal mechanisms. *Langmuir* 36, 9160–9174.
- Li, B., Liao, P., Liu, P., Wang, D., Ye, Z., Wang, J., et al., 2022. Formation, aggregation, and transport of NOM-Cr(III) colloids in aquatic environments. *Environ. Sci. Nano.* 9, 1133–1145.
- Li, B., Liao, P., Xie, L., Li, Q., Pan, C., Ning, Z., et al., 2020b. Reduced NOM triggered rapid Cr(VI) reduction and formation of NOM-Cr(III) colloids in anoxic environments. *Water Res.* 181, 115923.
- Li, Q., Xie, L., Jiang, Y., Fortner, J.D., Yu, K., Liao, P., et al., 2019. Formation and stability of NOM-Mn(III) colloids in aquatic environments. *Water Res.* 149, 190–201.
- Li, Y., Dong, S., Qiao, J., Liang, S., Wu, X., Wang, M., et al., 2020c. Impact of nanominerals on the migration and distribution of cadmium on soil aggregates. *J. Clean. Prod.* 262, 121355.
- Liao, P., Li, W., Jiang, Y., Wu, J., Yuan, S., Fortner, J.D., et al., 2017. Formation, aggregation, and deposition dynamics of NOM-iron colloids at anoxic-oxic interfaces. *Environ. Sci. Technol.* 51, 12235–12245.
- Liao, P., Pan, C., Ding, W., Li, W., Yuan, S., Fortner, J.D., et al., 2020. Formation and transport of Cr(III)-NOM-Fe colloids upon reaction of Cr(VI) with NOM-Fe(II) colloids at anoxic-oxic interfaces. *Environ. Sci. Technol.* 54, 4256–4266.
- Liu, L., Hu, S., Wu, C., Liu, K., Weng, L., Zhou, W., 2021a. Aggregates characterizations of the ultra-fine coal particles induced by nanobubbles. *Fuel* 297, 120765.
- Liu, M., Han, X., Liu, C.Q., Guo, L., Ding, H., Lang, Y., 2021b. Differences in the spectroscopic characteristics of wetland dissolved organic matter binding with Fe^{3+} , Cu^{2+} , Cd^{2+} , Cr^{3+} and Zn^{2+} . *Sci. Total Environ.* 800, 149476.
- Liu, Y., Huang, Z., Zhou, J., Tang, J., Yang, C., Chen, C., et al., 2020. Influence of environmental and biological macromolecules on aggregation kinetics of nanoplastics in aquatic systems. *Water Res.* 186, 116316.
- Lodygin, E.D., Alekseev, II., Vasilevich, R.S., Abakumov, E.V., 2020. Complexation of lead and cadmium ions with humic acids from arctic peat soils. *Environ. Res.* 191, 110058.
- Long, Y., Zhu, N., Zhu, Y., Shan, C., Jin, H., Cao, Y., 2024. Hydrochar drives reduction in bioavailability of heavy metals during composting via promoting humification and microbial community evolution. *Bioresour. Technol.* 395, 130335.
- Lucon, T.N., Costa, A.T., Galvao, P., Leite, M.G.P., 2020. Cadmium behavior in a karst environment hydrological cycle. *Environ. Sci. Pollut. Res.* 27, 8965–8979.
- Ma, J., Guo, H., Lei, M., Li, Y., Weng, L., Chen, Y., et al., 2018. Enhanced transport of ferrihydrite colloid by chain-shaped humic acid colloid in saturated porous media. *Sci. Total Environ.* 621, 1581–1590.
- Maurer, F., Christl, I., Hoffmann, M., Kretzschmar, R., 2012. Reduction and reoxidation of humic acid: influence on speciation of cadmium and silver. *Environ. Sci. Technol.* 46, 8808–8816.
- Meng, H., Hu, S., Hong, Z., Chi, W., Chen, G., Cheng, K., et al., 2024. Effects of zero-valent iron added in the flooding or drainage

- process on cadmium immobilization in an acid paddy soil. *J. Environ. Sci.* 138, 19–31.
- Meng, Q., Jin, L., Cheng, L., Fang, J., Lin, D., 2021. Release and sedimentation behaviors of biochar colloids in soil solutions. *J. Environ. Sci.* 100, 269–278.
- Myneni, S.C.B., Brown, J., Martinez, G., Meyer-Ilse, W.J.S., 1999. Imaging of humic substance macromolecular structures in water and soils. *Science* 286, 1335–1337.
- Ni, L., Li, D., Su, L., Xu, J., Li, S., Ye, X., et al., 2016. Effects of algae growth on cadmium remobilization and ecological risk in sediments of Taihu Lake. *Chemosphere* 151, 37–44.
- Nies, D.H., 2003. Efflux-mediated heavy metal resistance in prokaryotes. *FEMS Microbiol. Rev.* 27, 313–339.
- Opitz, J., Bauer, M., Alte, M., Schmidtmann, J., Peiffer, S., 2022. Sedimentation kinetics of hydrous ferric oxides in ferruginous, circumneutral mine water. *Environ. Sci. Technol.* 56, 6360–6368.
- Pan, Y., Ye, H., Yang, Y., Yang, C., Li, X., Ma, T., et al., 2023. Transport and fate of Cu and Cd in contaminated paddy soil under acid mine drainage. *J. Environ. Manage.* 334, 117517.
- Qu, C., Chen, J., Mortimer, M., Wu, Y., Cai, P., Huang, Q., 2022. Humic acids restrict the transformation and the stabilization of Cd by iron (hydr)oxides. *J. Hazard. Mater.* 430, 128365.
- Shams, M., Alam, I., Chowdhury, I., 2020. Aggregation and stability of nanoscale plastics in aquatic environment. *Water Res* 171, 115401.
- Shao, Z., Luo, S., Liang, M., Ning, Z., Sun, W., Zhu, Y., et al., 2021. Colloidal stability of nanosized activated carbon in aquatic systems: Effects of pH, electrolytes, and macromolecules. *Water Res* 203, 117561.
- Shen, X., Zhu, H., Wang, P., Zheng, L., Hu, S., Liu, C., 2022. Mechanistic and modeling insights into the immobilization of Cd and organic carbon during abiotic transformation of ferrihydrite induced by Fe(II). *J. Hazard. Mater.* 436, 129216.
- Sikder, M., Wang, J., Poulin, B.A., Tfaily, M.M., Baalousha, M., 2020. Nanoparticle size and natural organic matter composition determine aggregation behavior of polyvinylpyrrolidone coated platinum nanoparticles. *Environ. Sci. Nano.* 7, 3318–3332.
- Su, M., Liu, Z., Yuvaraja, G., Ou, T., Huang, Y., Hu, X., et al., 2020. The influence of particle size and natural organic matter on U(VI) retention by natural sand: Parameterization and mechanism study. *Sci. Total Environ.* 741, 140292.
- Su, X., Liu, J., 2017. pH-guided self-assembly of copper nanoclusters with aggregation-induced emission. *ACS Appl. Mater. Interfaces*. 9, 3902–3910.
- Tang, X.Y., Katou, H., Suzuki, K., 2020. Liming effects on dissolved and colloid-associated transport of cadmium in soil under intermittent simulated rainfall. *J. Hazard. Mater.* 400, 123244.
- Tiberg, C., Sjostedt, C., Gustafsson, J.P., 2018. Metal sorption to Spodosol Bs horizons: organic matter complexes predominate. *Chemosphere* 196, 556–565.
- Verwey, E.J.M., Overbeek, J.T.G., 1947. In: Theory of the Stability of Lyophobic Colloids, 51. Elsevier, Amsterdam, pp. 631–636.
- Wang, L.F., Wang, L.L., Ye, X.D., Li, W.W., Ren, X.M., Sheng, G.P., et al., 2013. Coagulation kinetics of humic aggregates in mono- and di-valent electrolyte solutions. *Environ. Sci. Technol.* 47, 5042–5049.
- Wang, M., Lu, T., Chen, W., Zhang, H., Qi, W., Song, Y., et al., 2020. Enhanced role of humic acid on the transport of iron oxide colloids in saturated porous media under various solution chemistry conditions. *Colloids Surf. A Physicochem. Eng. Asp.* 607, 125486.
- Wang, Z., Bian, Y., Xu, Y., Zheng, C., Jiang, Q., An, C., 2022. Artificial aging induced changes in biochars properties and Cd²⁺ adsorption behaviors. *Environ. Sci. Pollut. Res.* 30, 20133–20146.
- Wen, Z., Shang, Y., Song, K., Liu, G., Hou, J., Lyu, L., et al., 2022. Composition of dissolved organic matter (DOM) in lakes responds to the trophic state and phytoplankton community succession. *Water Res.* 224, 119073.
- Won, J., Wirth, X., Burns, S.E., 2019. An experimental study of cotransport of heavy metals with kaolinite colloids. *J. Hazard. Mater.* 373, 476–482.
- Wu, M., Bi, E., Li, B., 2022. Cotransport of nano-hydroxyapatite and different Cd(II) forms influenced by fulvic acid and montmorillonite colloids. *Water Res.* 218, 118511.
- Xu, M., Zhao, Z., Shi, M., Yao, L., Fan, T., Wang, Z., 2019. Effect of humic acid on the stabilization of cadmium in soil by coprecipitating with ferrihydrite. *Environ. Sci. Pollut. Res.* 26, 27330–27337.
- Yan, Y., Sun, Q., Yang, J., Zhang, X., Guo, B., 2021. Source attributions of Cadmium contamination in rice grains by Cadmium isotope composition analysis: a field study. *Ecotoxicol. Environ. Saf.* 210, 111865.
- Yang, J., Ge, M., Jin, Q., Chen, Z., Guo, Z., 2019a. Co-transport of U(VI), humic acid and colloidal gibbsite in water-saturated porous media. *Chemosphere* 231, 405–414.
- Yang, S., Wei, P., Wang, J., Tan, Y., Qu, X., 2023. Impacts of dissolved organic matter on the aggregation and photo-dissolution of cadmium pigment nanoparticles in aquatic systems. *Sci. Total Environ.* 865, 161313.
- Yang, W., Shang, J., Sharma, P., Li, B., Liu, K., Flury, M., 2019b. Colloidal stability and aggregation kinetics of biochar colloids: Effects of pyrolysis temperature, cation type, and humic acid concentrations. *Sci. Total Environ.* 658, 1306–1315.
- Yao, Y., Hu, X., Zhang, Y., He, H., Li, S., 2022. Visible light promoted the removal of tetrabromobisphenol A from water by humic acid-FeS colloid. *Chemosphere* 289, 133192.
- Yao, Y., Mi, N., He, C., Yin, L., Zhou, D., Zhang, Y., et al., 2020. Transport of arsenic loaded by ferric humate colloid in saturated porous media. *Chemosphere* 240, 124987.
- Yin, G., Tao, L., Chen, X., Bolan, N.S., Sarkar, B., Lin, Q., et al., 2021. Quantitative analysis on the mechanism of Cd²⁺ removal by MgCl₂-modified biochar in aqueous solutions. *J. Hazard. Mater.* 420, 126487.
- You, J.G., Tseng, W.L., 2019. Peptide-induced aggregation of glutathione-capped gold nanoclusters: A new strategy for designing aggregation-induced enhanced emission probes. *Anal Chim Acta* 1078, 101–111.
- Yun, S.W., Baveye, P.C., Kim, K.B., Kang, D.H., Lee, S.Y., Son, J., et al., 2016. Effect of postmining land use on the spatial distribution of metal(loids) and their transport in agricultural soils: Analysis of a case study of Chungyang, South Korea. *J. Geochem Explor* 170, 157–166.
- Zhang, H., Ji, Z., Chen, W., Pei, Y., 2024. Codisposal of landfill leachate concentrate and antimony mine soils using a one-part geopolymer system for cationic and anionic heavy metals immobilization. *J. Hazard. Mater.* 464, 132909.
- Zhang, L., Wang, X., Yue, D., 2020a. Effect of submerged combustion evaporation on Cd complexation potential of organic matter in municipal solid waste landfill leachate. *Environ. Pollut.* 267, 115573.
- Zhang, W., Ning, B., Sun, C., Song, K., Xu, X., Fang, T., et al., 2020b. Dynamic nano-Ag colloids cytotoxicity to and accumulation by Escherichia coli: Effects of Fe³⁺, ionic strength and humic acid. *J. Environ. Sci.* 89, 180–193.
- Zhao, X., Yuan, Z., Wang, S., Pan, Y., Chen, N., Tunc, A., et al., 2022. Iron(II)-activated phase transformation of Cd-bearing ferrihydrite: implications for cadmium mobility and fate under anaerobic conditions. *Sci. Total Environ.* 848, 157719.
- Zhong, X., Yang, Y., Liu, H., Fang, X., Zhang, Y., Cui, Z., et al., 2023. New insights into the sustainable use of soluble straw humic substances for the remediation of multiple heavy metals in contaminated soil. *Sci. Total Environ.* 903, 166274.
- Zhou, W., Ren, L., Zhu, L., 2017. Reducement of cadmium adsorption on clay minerals by the presence of dissolved

- organic matter from animal manure. *Environ. Pollut.* 223, 247–254.
- Zhou, Z., Muehe, E.M., Tomaszewski, E.J., Lezama-Pacheco, J., Kappler, A., Byrne, J.M., 2020. Effect of natural organic matter on the fate of cadmium during microbial ferrihydrite reduction. *Environ. Sci. Technol.* 54, 9445–9453.
- Zhu, P., Knoop, O., Helmreich, B., 2022a. Interaction of heavy metals and biocide/herbicide from stormwater runoff of buildings with dissolved organic matter. *Sci. Total Environ.* 814, 152599.
- Zhu, S., Mo, Y., Luo, W., Xiao, Z., Jin, C., Qiu, R., 2022b. Aqueous aggregation and deposition kinetics of fresh and carboxyl-modified nanoplastics in the presence of divalent heavy metals. *Water Res.* 222, 118877.